

# Patterning Flows Using Grooved Surfaces

Abraham D. Stroock,<sup>†</sup> Stephan K. Dertinger,<sup>†</sup> George M. Whitesides,<sup>†</sup> and Armand Ajdari<sup>\*,‡</sup>

Department of Chemistry and Chemical Biology, Harvard University, Cambridge Massachusetts 02138, and Laboratoire de Physico-Chimie Théorique, UMR CNRS-ESPCI 7083, 10 rue Vauquelin, F-75231 Paris Cedex 05, France

**Through a simple analytical description we quantify how pressure-driven flows over grooved surfaces develop transverse components, which, for shallow grooves, can be modeled with simple *anisotropic* effective boundary conditions. Helical recirculation results in channels or capillaries with grooved walls. An experimental validation of our model is presented. Our analysis provides a workable guide for the design of 3D flows with simple patterns of grooved regions, e.g., to control the position of streams in the cross section of a channel or to promote mixing. Potential applications in microfluidics are outlined.**

Currently, there is broad interest in methods for controlling the behavior of fluids in microsystems for potential use in small (hand-held), integrated devices for performing analytical and synthetic chemical tasks (see, for example, refs 1–3). Fluid handling for chemical applications typically requires elements such as pumps and valves<sup>2,4</sup> and also the ability to manipulate the position of streams within flows, e.g., for mixing<sup>5</sup> or for the spatially resolved delivery of reagents.<sup>6</sup> In microfluidic systems, it is a challenge to create the three-dimensional flows that are required for manipulating streams, because the Reynolds numbers are typically small ( $\leq 1$ ) and the channel geometries are typically long and narrow with pressure and electric fields applied from the ends. Another important practical constraint in designing microfluidic systems is that the common lithographic methods used in fabrication lead to planar, layered structures; complex three-dimensional structures are difficult to fabricate.<sup>7</sup> So in most microsystems, the flow structure follows locally a simple pattern, that is Poiseuille-like for pressure-driven flows, pluglike for electroosmotic flows (EOF), or a combination of both if recirculation constraints require it. Although some proposals exist for

generating more complex EO flows locally using heterogeneously charged surfaces,<sup>8–10</sup> pressure-driven flows have been largely limited to parabolic-like profiles.

In this paper, we propose a simple but general scheme to enlarge the forms of flow accessible with simple steady pressure gradients, taking advantage of the surface control allowed by microfabrication technology. Namely, we propose to create linear grooves on (at least) one of the surfaces of the channel, to make the surface locally anisotropic. This local anisotropy affects the overall geometry of the flow in a way that we analyze. Pressure-driven flows in these channels contain recirculating components that are transverse to the principle direction of flow. This recirculation can be used to mix adjacent streams, control the dispersion of plugs,<sup>5</sup> and position streams within the cross section of the channel. The simple model that we present in this paper should give experimentalists an accessible handle on the design of microfluidic components for such purposes.

To demonstrate the mechanism and provide estimates of the effects attainable, we focus here on the simplest pattern of a periodic set of parallel linear grooves. We consider first a slab geometry where the bottom wall has a sinusoidal profile of weak amplitude relative to the depth of the channel (Figure 1). In the section Flow over a Sinusoidally Modulated Surface we compute using a perturbation approach the pressure-driven flow in this geometry. This allows us to describe qualitatively and to estimate quantitatively the components of the flow generated transverse to an applied pressure gradient. Using this simple guide for describing the flows generated, we address in the section Flow Pattern in a Closed Channel the simple case of a channel of rectangular section with a floor bearing parallel grooves at an angle with respect to the channel axis and characterize the helical flow obtained. A first experimental check using microfabricated channels is reported in the section Experimental Check in Microfabricated PDMS Channels. We then conclude by discussing the extension to more complex patterns and applications, in microfluidics and in other domains.

Shear flows over grooved surfaces have been studied by a number of authors, many of whom were concerned with the role of the wall roughness on the effective boundary condition (slip

\* To whom correspondence should be addressed. E-mail: armand@turner.pct.espci.fr. Fax: 33-1-40-79-47-31.

<sup>†</sup> Harvard University.

<sup>‡</sup> Laboratoire de Physico-Chimie Théorique.

- (1) Stone, H. A.; Kim, S. *AIChE J.* **2001**, *47*, 1250–1254.
- (2) *Micro Total Analysis Systems 2000*; van den Berg, A., Olthuis, W., Bergveld, P., Eds.; Kluwer Academic Publishers: Dordrecht, The Netherlands, 2000.
- (3) Whitesides, G.; Stroock, A. D. *Phys. Today* **2001**, *54*, 42–48.
- (4) Unger, M. A.; Chou, H.; Thorsen, T.; Scherer, A.; Quake, S. R. *Science* **2000**, *288*, 113.
- (5) Stroock, A. D.; Dertinger, S.; Ajdari, A.; Mezic, I.; Stone, H. A.; Whitesides, G. *Science* **2002**, *295*, 647–651.
- (6) Takayama, S.; Ostuni, E.; LeDuc, P.; Naruse, K.; Ingber, D. E.; Whitesides, G. M. *Nature* **2001**, *411*, 1016.
- (7) Liu, R. H.; Stremier, M. A.; Sharp, K. V.; Olsen, M. G.; Santiago, J. G.; Adrian, R. J.; Aref, H.; Beebe, D. J. *J. Microelectromech. Syst.* **2000**, *9*, 190–197.

- (8) Stroock, A. D.; Weck, M.; Chiu, D. T.; Huck, W. T. S.; Kenis, P. J. A.; Ismagilov, R. F.; Whitesides, G. M. *Phys. Rev. Lett.* **2000**, *84*, 3314–3317. Erratum: *Phys. Rev. Lett.* **2001**, *86*, 6050.
- (9) Ajdari, A. *Phys. Rev. Lett.* **1995**, *75*, 755–758. Ajdari, A. *Phys. Rev. E* **1996**, *53*, 4996–5005.
- (10) Barker, S. L. R.; Ross, D.; Tavlov, M. J.; Gaitan, M.; Locascio, L. E. *Anal. Chem.* **2000**, *72*, 5925–5929.

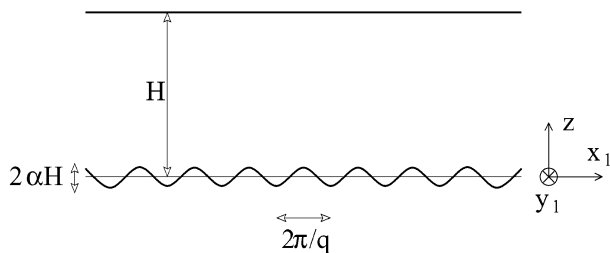


Figure 1. Geometry for the theoretical analysis presented.

or no-slip).<sup>11–13</sup> In these papers, grooves were taken as a simple representation of roughness (a 2D simplification of bumps), and only flow perpendicular to the grooves were analyzed. Here, we consider actual grooves, easily produced by microfabrication, and show that the effective boundary condition is tensorial and anisotropic. These anisotropic boundary conditions can then be used to understand the structure of the flow over grooves that are obliquely oriented with respect to the principle direction of flow. In particular, we present a simple formula for the magnitude of the net transverse component of the effective slip and for the structure of the recirculation that is generated in the fluid above a region of obliquely oriented grooves. These rules can be used to design complicated 3D flows for microfluidic applications.

#### FLOW OVER A SINUSOIDALLY MODULATED SURFACE

In this section, we calculate the pressure-driven flow between two parallel slabs, when one of them has a sinusoidal shape of small amplitude relative to the gap between the slabs. This is very similar to the work of Hocking<sup>12</sup> but for the fact that we insist on the surface being anisotropic (the grooves are not bumps, but extend—here indefinitely—in the  $y_1$  direction) and look for the consequences of this anisotropy.

For the sake of clarity, let us immediately specify our notation. We take the two planes to be perpendicular to the  $z$  axis and on average parallel to the  $(x_1, y_1)$  plane. More precisely, the location of the bottom modulated boundary is described by  $z^- = \alpha H \cos(qx_1)$  while the top flat one is located at  $z^+ = H$ . The wave vector of the sinusoidal modulation of the shape of the bottom plate is  $\mathbf{q} = q\mathbf{x}_1$ , while  $\alpha H$  is its amplitude, with  $\alpha$  a small nondimensional number.

We now solve the problem corresponding to steady low-Reynolds number hydrodynamics for an incompressible fluid of viscosity  $\eta$  (Stokes equation):

$$\eta \nabla^2 \mathbf{v} - \nabla p = \mathbf{0} \quad (1)$$

$$\nabla \cdot \mathbf{v} = 0 \quad (2)$$

where  $\mathbf{v}$  and  $p$  are the velocity and pressure fields, with no-slip boundary conditions on the top and bottom plates.

Here we focus more precisely on the flow generated by an applied pressure gradient in the  $(x_1, y_1)$  plane. If  $\alpha$  is zero, the flow has the simple Poiseuille form:

$$\mathbf{v}_0 = - (1/2\eta) z(H - z) \nabla p \quad (3)$$

For nonzero but small values of  $\alpha$ , it is possible to obtain a solution by a perturbative expansion in powers of  $\alpha$ . The simplest procedure owing to the linearity of the problem is to consider separately situations where the flow is parallel to  $x_1$  (and thus parallel to the modulation wave vector) and situations where flow is along  $y_1$  (and thus perpendicular to  $\mathbf{q}$ ).

Note that formally our calculation allows us to explore both the regime of distant plates  $qH \gg 1$ , where we expect the perturbation due to the grooves to generate effects localized to the vicinity of the surface, and the “lubrication” regime  $qH \ll 1$ , where the channel appears as a locally flat channel, with a height that changes slowly along  $x_1$ .

**A. Flow along  $x_1$ .** For pressure gradients and flow along  $x_1$ , the pressure gradient varies periodically along the direction  $x_1$ , and the flow has components along  $x_1$  and  $z$ . Solving eqs 1 and 2 with the no-slip boundary condition on  $z^-$  to second order in  $\alpha$ , we obtain

$$v_{x_1} = - \frac{H^2 \langle dp/dx_1 \rangle}{2\eta} \left[ \frac{z(H-z)}{H^2} - \frac{1}{2} \alpha^2 K_{||}(qH) \frac{H-z}{H} + T_{||}(x_1, z) \right] \quad (4)$$

where  $\langle dp/dx_1 \rangle$  is the position-independent pressure gradient averaged over a period along  $x_1$  and where  $T_{||}(x_1, z)$  are  $O(\alpha)$  and  $O(\alpha^2)$  terms periodic in  $x_1$ , of zero average, that correspond to structures (rolls) localized in the vicinity of the bottom plate in the case  $H \gg q^{-1}$  (see the Appendix for complete formulas).

Note that the  $z$  component of the flow is nonzero only in these rolls, where it can be obtained from the conservation equation  $\partial v_{x_1}/\partial x_1 + \partial v_z/\partial z = 0$  and the equation for  $T_{||}$  given in the Appendix. Elsewhere the flow is laminar  $\mathbf{v} = v_{x_1}(z)\mathbf{x}_1$ , with  $v_{x_1}$  given by eq 4.

The function  $K_{||}(qH)$  is given by

$$K_{||}(u) = -1 + 2u \frac{\sinh(u) \cosh(u) - u}{\sinh^2(u) - u^2} \quad (5)$$

so that in the lubrication limit  $qH \ll 1$ ,  $K_{||}(qH) \approx 3$ , and in the limit of plates very distant from one another  $H \gg q^{-1}$ ,  $K_{||}(qH \rightarrow \infty) \approx 2qH$ .

Another useful quantity is the total fluid flux between the two plates (per unit length in the  $y_1$  direction),  $J_{x_1} = \int_{z^-}^{z^+} v_{x_1} dz$ , which is a conserved quantity, and thus independent of  $x_1$ :

$$J_{x_1} = - \frac{H^3 \langle dp/dx_1 \rangle}{12\eta} \left[ 1 + \frac{3}{2} \alpha^2 (1 - K_{||}(qH)) \right] \quad (6)$$

Note that the periodic terms of eq 4 contribute as the boundary location  $z^-$  itself is also modulated. The addition of grooves increases the global resistance to flow by a term of order  $\alpha^2$  (from the symmetry of the problem, the sign of  $\alpha$  should not affect this average resistance, consistent with an even power in  $\alpha$ ).

**Effective Boundary Conditions.** With these equations in hand, let us pause to extract their physical message. We present two equivalent ways of accounting for the effect of the modulation

(11) Richardson, S. J. *Fluid Mech.* **1973**, *59*, 707–719.

(12) Hocking, L. M. J. *Fluid Mech.* **1976**, *76*, 801–817.

(13) Miksis, M. J.; Davis, S. H. *J. Fluid Mech.* **1994**, *273*, 125–139.

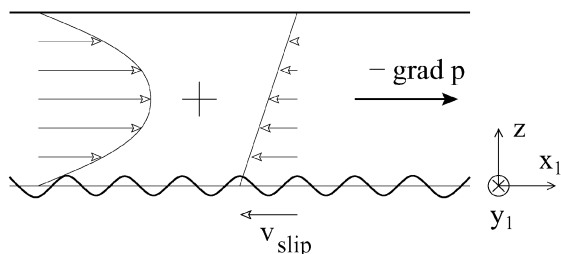


Figure 2. Effective slip velocity: the Poiseuille flow for a flat channel (left) modified due to the grooves on the bottom plate by a correction that takes the form of a simple shear flow (shown schematically, not to scale), plus periodic recirculation structures localized in the vicinity of the bottom plate (not shown).

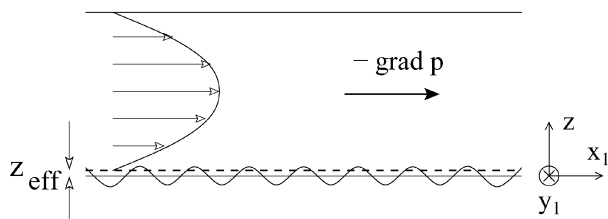


Figure 3. Alternative picture of the effect of the modulation. The net average flow is Poiseuille-like, but with an effective no-slip boundary condition located at  $z_{\text{eff}}$ .

of the surface shape by modified effective boundary conditions for the hydrodynamic problem. These are most meaningful when the gap  $H$  is much larger than the other lengths in the problem and in particular  $qH \gg 1$ .

The first perspective (see Figure 2) comes directly from eq 4, which indicates that the net (averaged over a period) result of the modulation of the bottom floor is an additional simple shear flow against the principle flow, which corresponds to an effective slip velocity  $v_{\text{slip}}$  on the reference  $z = 0$  plane of amplitude

$$v_{\text{slip}} = \alpha^2 \frac{H^2}{4\eta} \left\langle \frac{dp}{dx_1} \right\rangle K_{\parallel}(qH) \quad (7)$$

In the limit of very distant plates  $H \rightarrow \infty$ , this quantity should depend only on local quantities, i.e., not explicitly on  $H$ . In this limit, the local shear rate just above the (flat) bottom plate is  $\dot{\gamma} = -H/2\eta \langle dp/dx_1 \rangle$ , and  $K_{\parallel} = 2qH$ , so that  $v_{\text{slip}} = -q\dot{\gamma}(\alpha H)^2$ .  $v_{\text{slip}}$  is indeed only linked to local quantities: the local shear rate  $\dot{\gamma}$ , the amplitude  $\alpha H$ , and the wave vector  $q$  of the undulations. In this limit, the correction to the total flux  $J_{x_1}$  reads  $(H/2)v_{\text{slip}}$ , as it should given the no-slip boundary condition on the top plate (see eq 6).

In a second picture (see Figure 3), neglecting the periodic terms of zero average, eq 4 can be rewritten as a simple Poiseuille flow:

$$v_{x_1} = -\frac{1}{2\eta} \left\langle \frac{dp}{dx_1} \right\rangle (H-z)(z-z_{\text{eff}}) \quad (8)$$

which corresponds to a flat bottom no-slip surface located at

$$z_{\text{eff}} = \frac{1}{2} K_{\parallel}(qH) H \alpha^2 \quad (9)$$

This kind of boundary condition is often referred to as the “extrapolation length” or “slip length” in the literature describing slip phenomena over surfaces, i.e., the location at which the flow profile extrapolates to a no-slip boundary condition (usually  $-z_{\text{eff}}$  is what is called the extrapolation length). The positive value of  $z_{\text{eff}}$  (i.e., negative slip) again demonstrates that on average the grooves increase the friction due to the surface. In the  $qH \rightarrow \infty$  limit,  $z_{\text{eff}}$  is appropriately a local geometrical quantity independent of  $H$ :  $z_{\text{eff}} = q(\alpha H)^2$ . One can check that in this limit the flux obeys the corresponding Poiseuille (Hele–Shaw) formula  $J_{x_1} = -((H - z_{\text{eff}})^3/12\eta) \langle dp/dx_1 \rangle$ .

Although it carries exactly the same physics as the slip velocity picture, this “extrapolation length” description is a more intrinsic geometrical one, independent of the applied forces. In the  $qH \gg 1$  relevant limit, the two are simply (and logically) connected by  $v_{\text{slip}} = -\dot{\gamma} z_{\text{eff}}$ . The two pictures are usually captured by a so-called mixed boundary condition:

$$v_{x_1}|_{z=0} + z_{\text{eff}} \left. \frac{\partial v_{x_1}}{\partial z} \right|_{z=0} = 0 \quad (10)$$

Note that both pictures cannot be used so simply in the  $qH \rightarrow 0$  limit (narrow channels), as the effective terms appearing in the velocity field eq 4 and in the net flux eq 6 are then different.

Also note that, in the case of short-wavelength grooves, so that although  $\alpha \ll 1$  one still has  $\alpha qH \gg 1$  (grooves deeper than wide), it is clear from eq 4 that the expansion for the flow breaks down in the vicinity of the bottom surface (i.e., for  $z$  of order  $\alpha$ ) as the leading term scales as  $\alpha$  while the correction is of order  $\alpha^2 qH$  and thus larger! Other evidence of this breakdown is that eq 9 then predicts a value of  $z_{\text{eff}}$  that is larger than the groove height  $\alpha H$ . In this situation of deep narrow grooves, the flow penetrates inside the grooves only on a distance  $\sim 1/q$  due to the Laplacian nature of the equations, the driving shear being screened before it reaches the bottom. One then expects that the proper effective boundary condition is of the form  $z_{\text{eff}} \approx \alpha H - c/q$ , where  $c$  is a geometrical constant of order 1 (this is actually consistent with calculations in ref 12, which suggest  $c \approx 0.56$ ).

**B. Flow along  $y_1$ .** For pressure gradients and flow along  $y_1$ , the pressure gradient is constant, and the flow is uniaxial along  $y_1$  and varies periodically along the direction  $x_1$ . The flow (again to second order in  $\alpha$ ) has a structure formally similar to the one of eq 4:

$$v_{y_1} = -\frac{H^2}{2\eta} \left\langle \frac{dp}{dy_1} \right\rangle \left[ \frac{z(H-z)}{H^2} - \frac{1}{2} \alpha^2 K_{\perp}(qH) \frac{H-z}{H} + T_{\perp}(x_1, z) \right] \quad (11)$$

where  $T_{\perp}(x_1, z)$  again corresponds to terms periodic in  $x_1$ , of zero average, localized in the vicinity of the bottom plate in the case  $H \gg q^{-1}$  (formulas for these terms are given in the Appendix). Note that in this geometry there is strictly no component of the flow along  $z$ , the flow being laminar and along  $y_1$  uniquely.

The function  $K_{\perp}(qH)$  is given by

$$K_{\perp}(u) = -1 + u \frac{\cosh(u)}{\sinh(u)} \quad (12)$$

so that in the lubrication limit  $qH \ll 1$ ,  $K_{\perp}(qH) \approx (qH)^2/3$ , while

in the limit of plates distant from one another  $H \gg q^{-1}$ ,  $K_{\perp}(qH \rightarrow \infty) \simeq qH$ .

The fluid flux between the two plates now varies periodically with  $x_1$ , and its average reads

$$\langle J_{y_1} \rangle = -\frac{H^3}{12\eta} \left( \frac{dp}{dy_1} \right) \left[ 1 + \frac{3}{2} \alpha^2 (1 - K_{\perp}(qH)) \right] \quad (13)$$

Note that, in contrast to the previous case of flow perpendicular to the grooves, the average hydrodynamic resistance is reduced by the presence of the grooves for long-wavelength undulations (lubrication regime  $qH \ll 1$ ).

In the opposite limit  $qH \gg 1$  of a gap  $H$  large compared to the groove wavelength ( $qH \gg 1$ ), which is here our main focus, the grooves increase the overall hydrodynamic resistance, but by a factor weaker than in subsection A. Again the net effect appears as an effective slip on the bottom plate at

$$v_{\text{slip}\perp} = \alpha^2 \frac{H^2}{4\eta} \left( \frac{dp}{dy_1} \right) K_{\perp}(qH) \quad (14)$$

Alternatively, one can also consider that the bottom plate behaves as a flat one located at an “extrapolation length”

$$z_{\text{eff}\perp} = \frac{1}{2} K_{\perp}(qH) H \alpha^2 \quad (15)$$

a value smaller than the one for the parallel case (by a factor of order 2 for  $H \gg q^{-1}$ ).

**C. General Case: Transverse Effects.** An interesting point is of course that the “effective slips” generated along the two directions ( $x_1$ ,  $y_1$ ) are in general different. As a result of this anisotropy, if a pressure gradient is applied at some angle with respect to these two main directions, a sideways shear will develop, at a finite angle with respect to the applied gradient. Equivalently, through the “extrapolation length” picture, the gap appears wider for a flow parallel to the grooves (perpendicular to  $\mathbf{q}$ ), so that the flow slightly deviates from the direction of applied pressure gradient toward that of the “easy axis” of the system that is along the grooves. Formally, if both the depth and wavelength of the grooves are small compared to the characteristic dimensions of the flow along the surface ( $\alpha H$ ,  $q^{-1} \ll H$ ), the appropriate boundary condition is tensorial and mixed:

$$\mathbf{v}|_{z=0} + \mathbf{Z}_{\text{eff}} \frac{\partial \mathbf{v}}{\partial z} \Big|_{z=0} = \mathbf{0} \quad (16)$$

where  $\mathbf{Z}_{\text{eff}}$  is a  $2 \times 2$  tensor, diagonal in the ( $x_1$ ,  $y_1$ ) base with eigenvalues  $z_{\text{eff}\parallel}$  and  $z_{\text{eff}\perp}$ .

More quantitatively, for a pressure gradient applied at an angle  $\phi$  with the  $y_1$  direction, i.e., along  $\mathbf{Y} = \cos \phi \mathbf{y}_1 + \sin \phi \mathbf{x}_1$  (see Figure 4), the average flux can be written

$$\langle \mathbf{J} \rangle = -\frac{H^3}{12\eta} \left( \frac{dp}{dY} \right) \left[ \left[ 1 + \frac{3}{2} \alpha^2 (1 - K_{\parallel}) \right] \mathbf{Y} + \frac{3}{2} \alpha^2 (K_{\parallel} - K_{\perp}) \cos \phi \mathbf{y}_1 \right] \quad (17)$$

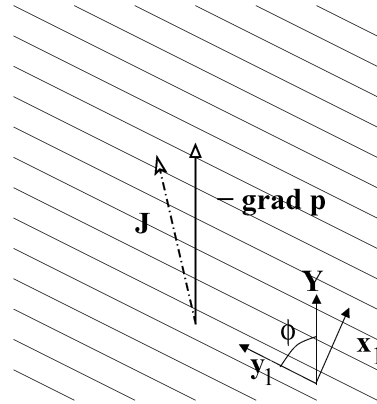


Figure 4. Top view of an infinite Hele–Shaw cell with grooves on the floor. A pressure gradient along  $\mathbf{Y}$  induces a fluid flux  $\mathbf{J}$  with a transverse component that tends to slightly align the flow along the grooves. This transverse effect can be viewed as generated by a sideways slip on the surface.

which clearly shows the two main effects of the modulation to order  $\alpha^2$ : a reduction of the amplitude of the main Poiseuille flow along the pressure gradient direction (recall that  $1 - K_{\parallel} < 0$ ) and the generation at the grooved surface of a sideways shear flow along  $y_1$  (recall that  $K_{\parallel} - K_{\perp} > 0$ ).

When is this effect noticeable? One may want to make the factor  $K_{\parallel}(qH) - K_{\perp}(qH)$  large by choosing  $qH \gg 1$ , so that  $K_{\parallel} - K_{\perp} \simeq qH$ . However, as explained in subsection A, one expects the effects to saturate for roughly  $qH \sim \alpha^{-1}$ , which makes the overall correction to the flux of order  $\alpha$ , the ratio of the groove depth  $\alpha H$  to the channel height  $H$ .

The transverse effect described here may lead to interesting boundary-controlled flow patterning: by changing the orientation of the modulation from place to place, one may generate various flow patterns from a single constant-pressure gradient (see, for example, ref 5), as the interaction of the various surface-induced shear flows will generate 3D recirculation structures so as to satisfy the incompressibility constraint. We claim that the above description in terms of slip velocity offers a very simple guide for predicting the geometry of the flows thus generated, as we will illustrate below for the case of a rather simple channel.

#### FLOW PATTERN IN A CLOSED CHANNEL

An important example we focus on is the case of a rectangular channel, with a grooved floor, and such that the grooves are at an angle  $\theta$  with respect to the axis of the channel  $\mathbf{y}_2 = \mathbf{x}_1 \sin \theta + \mathbf{y}_2 \cos \theta$  (see Figure 5). We take this patterned channel to be of thickness  $H$ , of width  $w$  in the  $x_2$  direction, and of length  $L$  much larger than all the above distances. We consider here the fully developed flow present in most of the channel. At the entrance and the exit of the patterned section, one expects the flow to evolve progressively from what it is before or after (i.e., Poiseuille-like) to this fully developed geometry over an induction length determined by vorticity diffusion over at least  $H$  and at most  $w$ . This length obviously depends on the average or typical flow velocity, whereas the shape of the fully developed flow does not in the limit of low Reynolds numbers.

Although an exact solution is beyond reach, we can gain insight with approximate solutions in the two following cases (which are not mutually exclusive). First, if the undulation wavelength  $q$  and

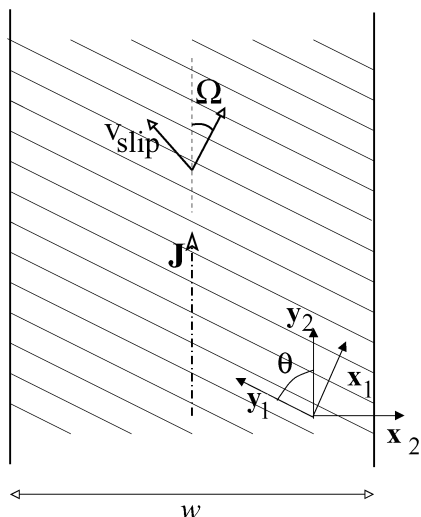


Figure 5. Top view of a channel of width  $w$  and main axis  $y_2$ . The undulation is at an angle  $\theta$  with this axis, so the circulation of a flux along the channel generates a slip  $v_{\text{slip}}$  on the bottom plate toward the left, schematically represented here. The presence of the side walls consequently leads to a positive pressure difference between the left and the right driving recirculation. As a result, the flow below the top surface is slightly biased toward the right, at an angle  $\Omega$  with the channel axis. The streamlines altogether are expected to have a helicoidal shape, following  $v_{\text{slip}}$  on the lowest part of the channel and recirculating at an angle  $\Omega$  in the top part.

amplitude  $\alpha H$  are much smaller than all the dimensions of the channel, we can adopt the above-mentioned concept of slip velocities. Second, if the channel is much wider than it is thick so that  $w \gg H, q^{-1}$ , then we can use the formulas of the preceding section to analyze the effectively 2D problem that results.

**A. Shallow Grooves.** When the amplitude of the undulation,  $\alpha H$ , is small compared to the channel thickness,  $H$ , the magnitude of the generated slip will be weak relative to the main Poiseuille-like flow in the channel. To get an estimate of the structure of the flow, a possible strategy is to take existing formulas for pressure-driven flows in rectangular channels and then calculate the local value of the shear rate  $\dot{\gamma}$  for each position  $x_2, y_2$  on the floor of the channel. As the zeroth-order flow is in the  $y_2$  direction, the resulting slip velocity will be  $v_{\text{slip}} = -q\dot{\gamma}(\alpha H)^2(\sin \theta \mathbf{x}_1 + 1/2 \cos \theta \mathbf{y}_1) = -q\dot{\gamma}(\alpha H)^2(1/2 \sin \theta \cos \theta \mathbf{x}_2 + (1 - 1/2 \cos^2 \theta) \mathbf{y}_2)$ . Then one should solve (probably using numerical methods) the flow generated by these slip boundary conditions. The main effect is of course that the component along  $\mathbf{x}_2$  will generate a slip toward a side wall so that a transverse pressure gradient will build up to drive the necessary recirculation of the fluid.

**B. Thin Channels.** In the case of shallow channels ( $w \gg H$ ), we can closely follow the general description in ref 14. In a thin channel bounded by side walls, the 2D fluxes (i.e., integrating over the  $z$  direction), are  $J_{y_2} = 0$  and  $J_{x_2} = cst = J$ , where these fluxes can be obtained by linear superposition of the quantities found in the previous section (eqs 6 and 13), by averaging over distances larger than  $1/q$ . Note that this procedure neglects the exact description of what happens in the vicinity of the lateral side walls, where over a width  $\sim H \ll w$  more intricate formulas would be needed.

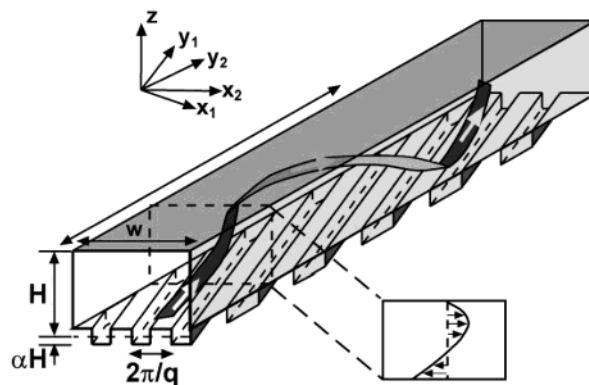


Figure 6. Schematic diagram of a microchannel with square grooves in the bottom wall. Below the channel to the right, the average flow profile in the cross section is drawn schematically. The ribbon indicates schematically a typical helicoidal streamline in the channel.

Of course, as in the preceding subsection, a transverse pressure gradient will build up to ensure that  $J_{x_2} = \cos \theta J_{x_1} - \sin \theta J_{y_1}$  is zero. This allows us to determine  $\langle \partial_{x_1} p \rangle$  and  $\partial_{y_1} p$  as functions of the constant  $J_{y_2} = J$ . With these known, it is simple to use (4) and (11) to obtain the flow profile in the horizontal plane to order  $\alpha^2$ :

$$\mathbf{v} = \frac{6J}{H} \left( 1 - \frac{3}{2} \alpha^2 \right) \left[ \frac{z(H-z)}{H^2} \right] \mathbf{y}_2 + \alpha^2 \frac{6J}{H} \left[ \frac{3}{2} \frac{z(H-z)}{H^2} - \frac{H-z}{2H} \right] \times (K_{\parallel} \sin \theta \mathbf{x}_1 + K_{\perp} \cos \theta \mathbf{y}_1) + \text{periodic terms} \quad (18)$$

This expression shows that the net flux is along  $\mathbf{y}_2$  as the second term on the rhs carries no net flux, with the flux of the shear flow due to the slip velocity compensated by a Poiseuille recirculation flow. This term appears in addition to the Poiseuille flow along the axis of the channel, the amplitude of which is slightly reduced as a consequence of the modulation.

Together these two terms correspond to a helicoidal pattern of the streamlines (similar to the sketch in Figure 6), with an apparent slip of the fluid on the bottom floor at  $v_{\text{slip}} = (3\alpha^2 J/H) \cdot (K_{\parallel} \sin \theta \mathbf{x}_1 + K_{\perp} \cos \theta \mathbf{y}_1)$ .

An alternative way to write the flow is

$$\mathbf{v} = \frac{6J}{H} \left( 1 - \frac{3}{2} \alpha^2 (1 - \bar{K}) \right) \left[ \frac{(H-z)(z - \bar{z}_{\text{eff}})}{H^2} \right] \mathbf{y}_2 + \alpha^2 \frac{6J}{H} \left[ \frac{3}{2} \frac{z(H-z)}{H^2} - \frac{H-z}{2H} \right] (K_{\parallel} - K_{\perp}) \sin \theta \cos \theta \mathbf{x}_2 + \text{periodic terms} \quad (19)$$

where  $\bar{K}$  and  $\bar{z}_{\text{eff}}$  are averages of their  $\parallel$  and  $\perp$  counterparts:  $\bar{K} = K_{\parallel} \sin^2 \theta + K_{\perp} \cos^2 \theta$  and  $\bar{z}_{\text{eff}} = z_{\text{eff}\parallel} \sin^2 \theta + z_{\text{eff}\perp} \cos^2 \theta$ . Again eq 19 describes a Poiseuille-like flow along the channel (with an effective bottom boundary) plus a transverse recirculation corresponding to a slip along  $\mathbf{x}_2$  of magnitude  $-(3\alpha^2 J/H)(K_{\parallel} - K_{\perp}) \sin \theta \cos \theta \mathbf{x}_2$ . Equation 19 clearly shows that the existence of this transverse slip and recirculation relies on the difference between  $K_{\parallel}$  and  $K_{\perp}$  and vanishes if the channel axis coincides with one of the principal axis of the modulation ( $\theta = 0$  or  $\theta = \pi/2$ ).

A measure of the helicity of the flow can be obtained from the last equation in the following way. If one analyzes the rate of shear

(14) Ajdari, A. *Phys. Rev. E* **2002**, *65*, 016301.



Figure 7. Optical micrograph taken from above of a stream of black dye flowing in a microchannel such as the one shown in Figure 6.  $w = 200 \mu\text{m}$ ,  $H = 79 \mu\text{m}$ ,  $q = 2\pi/100 \mu\text{m}$ , and  $\alpha = 0.34$ . The drawing on the left shows schematically the Y junction at the entrance of the channel; a narrow stream of black dye in water is injected alongside a broad stream of clear water (flow rate of the clear stream 20 times that of the dyed one). The average flow speed in the channel is 1 cm/s (Reynolds number  $Re \sim 1$ ). The pitch of the helical streamlines in the flow, as measured by the angle  $\Omega$ , is evaluated as shown by the dashed lines.

just below the flat top plate, the ratio of the components along  $x_2$  and along  $y_2$  provides a measure of the tangent of the angle  $\Omega$  between the flow there and the axis of the channel. This tangent is given by

$$\tan(\Omega) = \frac{\alpha^2(K_{\parallel}(qH) - K_{\perp}(qH)) \cos \theta \sin \theta}{1 - \alpha^2(3/2 - \tilde{K}(qH))} \quad (20)$$

This result is expected to be strictly valid in the combined limit of  $\alpha \ll 1$  and  $\alpha qH \ll 1$ , but may hold as a reasonable guide to provide an order of magnitude estimate even when the inequalities are not so strict. Actually, following the discussion in subsection C of the previous section, we anticipate that, for a given value  $\alpha H$  for the groove depth, the maximum effect corresponds to  $\alpha qH \sim 1$ , so that a rough estimate of the largest angle obtainable is

$$\tan(\Omega)|_{\max} \approx \alpha \cos \theta \sin \theta \quad (21)$$

#### EXPERIMENTAL CHECK IN MICROFABRICATED PDMS CHANNELS

We fabricated microchannels with grooves in one wall in order to test the prediction in eq 20 of the pitch of the trajectories in a channel flow over obliquely oriented undulations. (The general form of the channels is shown schematically in Figure 6.) We fabricated the channels in poly(dimethylsiloxane), a clear elastomeric polymer. We used methods described elsewhere.<sup>15</sup> Briefly, we made master structures with two-step photolithography in SU-8: The first layer of photolithography defined a positive image of our channel structure; the second layer defined a positive image of the pattern of ridges. The pattern was aligned to lie on top of the channel structure in the first layer. We measured the dimensions of the channel and the undulations using a profilometer. We made molds of the positive structure in PDMS. To close the channel, we exposed the PDMS to a plasma for 1 min and sealed it to a glass slide.

To evaluate the pitch of trajectories, we injected a narrow stream of a dye solution along one side of the channel as shown in Figure 7; a broader stream of clear solution was injected alongside the dyed stream. The flow rates of the two streams were imposed with a syringe pump. The clear stream was driven at 20 times the flow rate of the dyed stream by using syringes of

Table 1. Predicted and Measured Values of the Pitch ( $\tan \Omega$ ) of the Helical Trajectories in a Channel with Square Grooves on the Floor<sup>a</sup>

geometrical parameters	$\tan(\Omega) (\times 100)$	
	predicted	measured
$H = 79; qH = 5; \alpha = 0.134$	4.1	6.0
$H = 103; qH = 6.5; \alpha = 0.17$	7.7	6.4
$H = 67; qH = 4.2; \alpha = 0.20$	7.5	7.5
$H = 74; qH = 4.6; \alpha = 0.24$	11.1	8.8
$H = 79; qH = 5.0; \alpha = 0.34$	18.0	16.8
$H = 75; qH = 2.4; \alpha = 0.10$	1.5	2.4
$H = 69; qH = 2.2; \alpha = 0.20$	5.8	6.6
$H = 82; qH = 2.6; \alpha = 0.26$	9.6	10.0
$H = 87; qH = 2.7; \alpha = 0.37$	17.8	16.1

<sup>a</sup> In all cases  $w = 200 \mu\text{m}$ ,  $H$  is given in micrometers, and the grooves are oriented at an angle  $\theta = \pi/4$  with respect to the principal axis of the channel. Predicted values are obtained using formula 20 for sinusoidal grooves; experimental values are evaluated as described in Figure 7 (flow rate of the clear stream fixed to 20 times that of the dyed one,  $Re \sim 1$ ).

different diameters. The first millimeter of channel after the junction was flat (no grooves), which allowed the setting in of a steady Poiseuille profile with the dyed liquid confined to a narrow stream on the side of the channel. As the flow entered the patterned area, the narrow stream of dye was convected across the top of the channel, so that it occupied the region just below the ceiling of the channel. Consequently, this procedure allowed us to measure  $\tan(\Omega)$  as defined in eq 20, using optical micrographs like the one in Figure 7. The predicted (eq 20) and measured values of  $\tan(\Omega)$  are given in Table 1 for a few different values of  $qh$  and  $\alpha$ .

The predictions are qualitatively correct for  $\alpha < 0.3$ . In all cases, the order of magnitude is correct and so are the trends in terms of variations with the parameters  $\alpha$  and  $qH$ . Deviations of the absolute values may be due to the fact that the grooves are squared and not sinusoidal, that  $\alpha qH$  is often of order 1, which limits the validity of the perturbative expansion, and that the aspect ratio  $w/H$  of the channels is not very large, which makes the measurement of  $\Omega$  difficult and may slightly compromise the accuracy of our model that is based on a wide, thin channel. Note that we observe qualitatively the same flow for all  $Re < 100$ .

#### DISCUSSION

Using a simple perturbation approach, we have shown that the anisotropy of groove patterns on a wall allows one to engineer the flow in its vicinity, in a way that can be understood using effective slip boundary conditions. Owing to the necessary recirculation imposed by other boundaries, this slip leads to 3D flows. We then experimentally demonstrated this type of flow in a simple geometry, namely, a rectangular channel with a grooved floor. We have also provided simple tools that permit semiquantitative predictions of the effects to be expected.

To quantify more precisely the effects obtainable, much remains to be done, both numerically (CFD) and experimentally, to explore further the exact structures of flow for grooves of various depth and aspect ratio. An optimization of the shape of the grooves could come out of such studies.

More interesting is probably the exploration of the 3D flows generated by various 2D patterns of grooves. A grooved section

(15) McDonald, J. C.; Duffy, D. C.; Anderson, J. R.; Chiu, D. T.; Wu, H.; Schueller, O. J. A.; Whitesides, G. M. *Electrophoresis* **2000**, *21*, 27–40.

in a simple rectangular channel can induce swapping of the flow lines located in the vicinity of each of the side walls. Patches of parallel grooves with perpendicular “axes” allow the generation of parallel counter-rotating helices. We have shown that a periodic structure with staggered herringbone-shaped grooves generates Lagrangian chaos at low Reynolds number.<sup>5</sup> This flow can be used to speed up mixing in microfluidic devices. How designed flows over patterned surfaces influence exchanges of heat or matter between the surface and the bulk is also an interesting topic.

Although we have focused here on pressure-driven flows, electroosmotic flows can also be designed using either shape or charge patterns (or both), which could be of importance in microfluidics systems.<sup>14,16</sup>

It is important to emphasize that this exploration is not just a theoretical fancy, as the patterning of surfaces proposed here is compatible with planar lithography. These flows can thus not only be experimentally tested but also easily and quickly implemented in a parallel fashion either at many places on the same (macroscopic) surface or on many devices.

#### APPENDIX

For the sake of completeness, we give here the complete formula of the sinusoidal terms omitted in eqs 4 and 11. The periodic terms corresponding to a flow along  $x_1$ , i.e., perpendicular to the grooves read

$$T_{\parallel}(x_1, z) = -\alpha \frac{dg_q}{dz}(z) \cos(qx_1) + \frac{1}{2}\alpha^2 \frac{dh_q}{dz}(z) \cos(2qx_1) \quad (22)$$

with

(16) Johnson, T. L.; Ross, D.; Locascio, L. E. *Anal. Chem.* **2002**, *74*, 45–51.

$$g_q(z) = \frac{\sinh(qH)z \sinh(q(H-z)) - qH(H-z) \sinh(qz)}{\sinh(qH)^2 - (qH)^2} \quad (23)$$

$$h_q(z) = -K_{\parallel}(qH)g_{2q}(z) + (H/2)I_{2q}(z) \quad (24)$$

$$I_q(z) = [\sinh(qH) \sinh(q(H-z)) - qH \sinh(qz) + \sinh(qH)qz \cosh(q(H-z)) - qHq(H-z) \cosh(qz)] \times [\sinh(qH)^2 - (qH)^2]^{-1} \quad (25)$$

For the flow along  $y_1$ , we obtain

$$T_{\perp}(x_1, z) = -\alpha \frac{\sinh(q(H-z))}{\sinh(qH)} \cos(qx_1) - \frac{1}{2}\alpha^2 K_{\perp}(qH) \frac{\sinh(2q(H-z))}{\sinh(2qH)} \cos(2qx_1) \quad (26)$$

#### ACKNOWLEDGMENT

We thank Professor Howard Stone (Division of Engineering and Applied Sciences, Harvard University) for continuous interaction and exchanges on this and related topics. A.D.S., S.K.D. and G.M.W. acknowledge financial support from Defense Research Project Agency grant NSF ECS-9729405, Materials Science and Engineering Center grant NSF DMR-9807363, and NIH grant GM515. A.A. acknowledges support from an “ACI blanche” grant from the Ministère de la Recherche.

Received for review April 26, 2002. Accepted August 6, 2002.

AC0257389